ISSN 1674-1056
http://cpb.iphy.ac.cn
http://iopscience.iop.org/cpb
中国物理 B
Chinese Physics
中国物理 Chinese Physics B

Two-dimensional XSe_2 (X=Mn, V) based magnetic tunneling junctions with high Curie temperature

Longfei Pan(潘龙飞), Hongyu Wen(文宏玉), Le Huang(黄乐), Long Chen(陈龙), Hui-Xiong Deng(邓惠雄), Jian-Bai Xia(夏建白), Zhongming Wei(魏钟鸣)
Citation: Chin. Phys. B . 2019, 28(10): 107504 . **doi:** 10.1088/1674-1056/28/10/107504
Journal homepage: http://cpb.iphy.ac.cn; http://iopscience.iop.org/cpb

What follows is a list of articles you may be interested in

Magnetism induced by Mn atom doping in SnO monolayer

Ruilin Han(韩瑞林), Yu Yan(闫羽)
Chin. Phys. B . 2018, 27(11): 117505 . **doi:** 10.1088/1674-1056/27/11/117505

Ferromagnetism and magnetostructural coupling in V-doped MnNiGe alloys

Hui Yang(杨慧), Jun Liu(刘俊), Chao Li(李超), Guang-Long Wang(王广龙), Yuan-Yuan Gong(龚元元), Feng Xu(徐锋)
Chin. Phys. B . 2018, 27(10): 107502 . **doi:** 10.1088/1674-1056/27/10/107502

Progress of novel diluted ferromagnetic semiconductors with decoupled spin and charge doping: Counterparts of Fe-based superconductors

Shengli Guo(郭胜利), Fanlong Ning(宁凡龙)
Chin. Phys. B . 2018, 27(9): 097502 . **doi:** 10.1088/1674-1056/27/9/097502

Magnetic properties of AlN monolayer doped with group 1A or 2A nonmagnetic element: First-principles study

Ruilin Han(韩瑞林), Xiaoyang Chen(陈晓阳), Yu Yan(闫羽)
Chin. Phys. B . 2017, 26(9): 097503 . **doi:** 10.1088/1674-1056/26/9/097503

Effects of Zr substitution on structural, morphological, and magnetic properties of bismuth iron oxide phases

A Asif, M Hassan, S Riaz, S Naseem, S S Hussain
Chin. Phys. B . 2017, 26(8): 087502 . **doi:** 10.1088/1674-1056/26/8/087502

SPECIAL TOPIC — A celebration of the 100th birthday of Kun Huang

Two-dimensional XSe_2 (X = Mn, V) based magnetic tunneling junctions with high Curie temperature*

Longfei Pan(潘龙飞)[1], Hongyu Wen(文宏玉)[1,†], Le Huang(黄乐)[2], Long Chen(陈龙)[3], Hui-Xiong Deng(邓惠雄)[1], Jian-Bai Xia(夏建白)[1,4], and Zhongming Wei(魏钟鸣)[1,4,‡]

[1] State Key Laboratory of Superlattices and Microstructures, Institute of Semiconductors, Chinese Academy of Sciences & College of Materials Science and Opto-Electronic Technology, University of Chinese Academy of Sciences, Beijing 100083, China

[2] School of Materials and Energy, Guangdong University of Technology, Guangdong 510006, China

[3] Tianjin Key Laboratory of Molecular Optoelectronic Science, Department of Chemistry, Tianjin University, Tianjin 300072, China

[4] Beijing Academy of Quantum Information Sciences, Beijing 100193, China

(Received 13 August 2019; revised manuscript received 25 August 2019; published online 28 August 2019)

Two-dimensional (2D) magnetic crystals have attracted great attention due to their emerging new physical phenomena. They provide ideal platforms to study the fundamental physics of magnetism in low dimensions. In this research, magnetic tunneling junctions (MTJs) based on XSe_2 (X = Mn, V) with room-temperature ferromagnetism were studied using first-principles calculations. A large tunneling magnetoresistance (TMR) of 725.07% was obtained in the MTJs based on monolayer $MnSe_2$. Several schemes were proposed to improve the TMR of these devices. Moreover, the results of our non-equilibrium transport calculations showed that the large TMR was maintained in these devices under a finite bias. The transmission spectrum was analyzed according to the orbital components and the electronic structure of the monolayer XSe_2 (X = Mn, V). The results in this paper demonstrated that the MTJs based on a 2D ferromagnet with room-temperature ferromagnetism exhibited reliable performance. Therefore, such devices show the possibility for potential applications in spintronics.

Keywords: two-dimensional material, magnetic tunneling junctions, tunneling magnetoresistance, ferromagnetism

PACS: 75.70.Cn, 75.70.Ak, 68.65.–k **DOI:** 10.1088/1674-1056/ab3e45

1. Introduction

In the field of spintronics, magnetic tunneling junctions have been an important concern for researchers. MTJs with MgO, Al_2O_3, or organic molecules acting as tunneling barrier materials have been extensively studied.[1–3] Two-dimensional (2D) materials are widely studied for their novel properties and various advantages.[4–7] 2D materials provide a reliable solution to the problems in the manufacturing of high-performance MTJs through the layer-by-layer control of the thickness, sharp interfaces, and high perpendicular magnetic anisotropy (PMA).[8–10] In 2007, Karpan *et al.* first reported MTJs with a graphene layer as the barrier layer.[11] Another two-dimensional material, hexagonal boron nitride (h-BN) acting as an insulator with a similar structure to graphene, has been used as a barrier layer in MTJs.[12,13] Piquemal-Banci *et al.* investigated the electronic properties and performance of Co/h-BN/Fe MTJs[14] where the h-BN was directly grown by the chemical vapor deposition (CVD) method on pre-patterned Fe stripes. The authors reported TMR = 50% for their Co/h-BN/Fe MTJs. In addition, some MTJs using transition metal dichalcogenides (TMDC) as a barrier have recently been reported.[15,16]

Lately, great progress has been made in the research of 2D ferromagnetic materials.[17–22] Experimental advances have shown that ferromagnetic order can persist in monolayer CrI_3. Atomically thin CrI_3 flakes with intrinsic ferromagnetism were mechanically exfoliated from bulk material by Huang *et al.*[17] The material had a Curie temperature (T_C) of 45 K, and it had perpendicular magnetic anisotropy. Subsequently, another 2D metal, Fe_3GeTe_2, with intrinsic ferromagnetism, was reported to have a higher Curie temperature of 205 K and perpendicular magnetic anisotropy.[23] Wafer-scale two-dimensional Fe_3GeTe_2 thin films has been grown by molecular beam epitaxy.[24] Moreover, a typical TMR effect was observed in the Fe_3GeTe_2/h-BN/Fe_3GeTe_2 heterojunction.[25] However, the Curie temperature (T_C) in these monolayer ferromagnets was much lower than room temperature, and the ferromagnetic layered material was much desired. Recently, VSe_2 monolayers with room-temperature (300 K) ferromagnetism were synthesized by molecular beam epitaxy

*Project supported by the National Natural Science Foundation of China (Grant Nos. 61571415 and 61622406), the National Key Research and Development Program of China (Grant No. 2017YFA0207500), the Strategic Priority Research Program of the Chinese Academy of Sciences (Grant No. XDB30000000), and Beijing Academy of Quantum Information Sciences, China (Grant No. Y18G04).

†Corresponding author. E-mail: wenhongyu@semi.ac.cn

‡Corresponding author. E-mail: zmwei@semi.ac.cn

© 2019 Chinese Physical Society and IOP Publishing Ltd

(MBE).[26] Another group also reported $MnSe_2$ monolayers with room-temperature (300 K) ferromagnetism and perpendicular magnetic anisotropy on a specific substrate.[27,28]

Room-temperature ferromagnetism and perpendicular magnetic anisotropy are crucial for industrial applications in magnetic memory. In our calculations, single-layer h-BN was used as the barrier layer, and XSe_2 was used as the ferromagnetic layer. TMR is defined as the normalized difference between the resistances calculated in parallel spin states and anti-parallel spin states. The TMR is normally expressed as $\mathrm{TMR} = \frac{R_{\mathrm{AP}}-R_{\mathrm{P}}}{R_{\mathrm{P}}}$. R_{P} and R_{AP} are the resistances in parallel configurations and antiparallel configurations. For the convenience of our calculation, this equation was transformed into $\mathrm{TMR} = \frac{G_{\mathrm{P}}-G_{\mathrm{AP}}}{G_{\mathrm{AP}}}$, where G_{P} and G_{AP} are the conductance through the junction with parallel spin alignment and antiparallel spin alignment. Two approaches were proposed to improve the TMR of our MTJs: (i) choosing suitable electrodes and (ii) increasing the number of layers of the h-BN barrier layer finitely. From the local density of states of the $MnSe_2$/h-BN/$MnSe_2$ heterojunction, a barrier introduced by h-BN was clearly shown. We proposed new magnetic tunneling junctions that were based on materials with room-temperature ferromagnetism. This increased the working temperature of the MTJs based on a 2D ferromagnet to a room temperature of 300 K. We proposed new magnetic tunneling junctions that were based on materials with room-temperature ferromagnetism. This increased the working temperature of the MTJs based on a 2D ferromagnet to a room temperature of 300 K.

2. Computational methods

The device simulation in this work was performed using the first-principles software package ATOMISTIX TOOLKIT, which is based on density functional theory and non-equilibrium Green's function.[29] The exchange–correlation potential is described by gradient approximation with a Hubbard U parameter (GGA + U) approach. Hubbard term is normally defined as[30]

$$E_U = \frac{U}{2}\sum_{\sigma}\left[\left(\sum_{m1} n^{\sigma}_{m1,m1}\right) - \left(\sum_{m1,m2} n^{\sigma}_{m1,m2} n^{\sigma}_{m2,m1}\right)\right], \quad (1)$$

where m_1 and m_2 represent the projection of the d electrons orbital momentum ($m_1, m_2 = -2, -1, 0, 1, 2$), and σ represents spin states. The U value was obtained by a linear response method,[31] and the calculation was performed by Quantum-ESPRESSO (QE).[32] A cutoff energy of 100 Hartree was used for the plane-wave basis set. All the atoms and the lattice constants were fully relaxed until the force on each atom is less than 0.01 eV/Å. DFT-D2 method was used to consider Van der Waals force.[33] The Monkhorst–Pack k-point samplings for transport calculations was $2 \times 3 \times 200$ in the a, b, and c directions. The transport direction was along the c direction. The projector augmented wave (PAW) method and planewave basis set as implemented in the Vienna *ab-initio* simulation package (VASP) was used in electronic structure calculations.[34,35] The exchange–correlation energy was described by the generalized gradient approximation PBE (GGA-PBE) formalism.[36,37] In the PDOS calculations, a k-point sampling of $11 \times 11 \times 1$ was employed. The cutoff energy is 400 eV. Through Landauer conductance formula, conductance can be calculated as[38]

$$G_{\sigma} = \frac{e^2}{h}\sum_{k_{\parallel},j} T^{+}(k_{\parallel}, j), \quad (2)$$

$$G = G_{\uparrow} + G_{\downarrow}, \quad (3)$$

where σ is the spin index, j represents the Bloch state index, and $k_{\parallel}$ is the k-points used in the calculation. $T^{+}(k_{\parallel}, j)$ is the transmission coefficient. The superscript in $T^{+}(k_{\parallel}, j)$ indicates that the direction of transmission is from the left electrode to the right electrode.

3. Results and discussion

The schematic diagram of $MnSe_2$/h-BN/$MnSe_2$ MTJs is shown in Fig. 1(a). The monolayer $MnSe_2$ in the 1-T phase was used as the ferromagnetic layer.[27] Monolayer h-BN was employed as the barrier layer. In this research, we used Ir and Ru as the metal electrodes. Compared with metals such as gold, silver, and copper, Ir and Ru have a smaller lattice mismatch with XSe_2. The device configuration is shown in Fig. 1(a). The lengths of the left and right electrodes in our simulations exceed 7 Å.

On each side, the length of our screening region is approximately 11 Å, which guarantees the sufficient accuracy of the self-consistent calculation. The MTJs in this research did not contain the pinning layer because of the limitation of the computation amount. Our simulations could qualitatively illustrate the performance of these MTJs. The GGA + U method was used with $U = 3.71$ eV for $MnSe_2$ and $U = 3.93$ eV for VSe_2, which matches other groups' results well.[39] The detailed computational methods can be found in the methods section. The transmission spectrum of the $MnSe_2$/h-BN/$MnSe_2$ MTJs was calculated. As shown in Fig. 1, the magnitude of the transmission in a parallel magnetization configuration (PC) was one order of magnitude larger than the transmission in an antiparallel magnetization configuration (APC). This indicates that the MTJs had an apparent TMR effect. The transmission spectrum in Figs. 1(d) and 1(e) is like a superposition of the transmission spectrum in PC for the majority and minority spin states.

Through symmetry properties, d orbital component could be distinguished as $\Delta_1(\mathrm{d}_{z^2})$, $\Delta_5(\mathrm{d}_{xz}\mathrm{d}_{yz})$, $\Delta_2(\mathrm{d}_{x^2-y^2})$, and

$\Delta_{2'}(d_{xy})$.[40] As shown in Figs. 1(b) and 1(c), no dominant Δ_1 hot spot tunneling feature was observed in the reciprocal lattice vector $k_{\|}$-resolved transmission spectrum. The hotspots in Figs. 1(b) and 1(c) are not at the center but close to the corner. The transmission coefficient of the hot spots of Fig. 1(b) is 1.33, corresponding to $k_{\|} = (-0.41\pi/a, -0.47\pi/b)$ and $k_{\|} = (0.41\pi/a, 0.47\pi/b)$. The transmission coefficient of the hot spots of Fig. 1(c) is 0.26, corresponding to $k_{\|} = (-0.13\pi/a, 0.23\ \pi/b)$ and $k_{\|} = (0.13\pi/a, -0.23\pi/b)$. As shown in Fig. S2(a) in the supplementary material, the transmission eigenstate of the majority spin states in the PC has four nodes, which shows an obvious d-electron feature. As shown in Fig. 3(a), the d_{xz}, d_{yz}, $d_{x^2-y^2}$, and d_{xy} states of the single-layer $MnSe_2$ span across the Fermi level. The symmetry of these four d states belongs to (Δ_5, Δ_2, or $\Delta_{2'}$), which has horizontal momentum. Due to the horizontal momentum of these d-state electrons, $k_{\|}$ of the hot spots was not zero. The transmission spectrum in Fig. 1(c) has a fairly average transmission. The transmission characteristics of the hot spots have the characteristics of the d-state electrons, which had horizontal momentum. It can be seen from Fig. S2(b) in the supplementary material that the transmission eigenstate of the minority spin channel in PC was similar to a mixture of the s-states and d-states of Ru and the d-states of Mn. This could explain why the transmission of the transmission spectrum in Fig. 1(c) is fairly average. It is a mixture of transmissions of multiple electronic states with different symmetries. Compared to traditional MTJs, the total conductance of our calculated MTJs was larger by several orders of magnitude.[41]

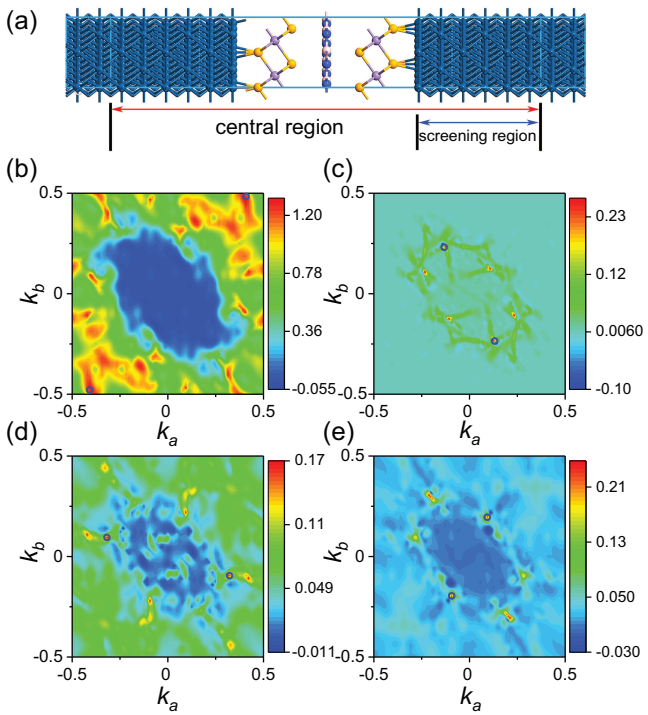


Fig. 1. (a) The configuration of Ru/$MnSe_2$/h-BN/$MnSe_2$/Ru MTJs. $k_{\|} = (k_a, k_b)$ dependent transmission spectra of MTJs based on $MnSe_2$ for the (b) majority spin channel and (c) minority spin channel in PC, and (d) the majority spin channel and (e) minority spin channel in APC. The blue circles mark the hottest spots in each figure.

The transmission spectrum of VSe_2/h-BN/VSe_2 MTJs is shown in Fig. 2. The hot spots in Fig. 2(a) are $k_{\|}$ = (0.45 π/a, 0.33 π/b) and $k_{\|} = (-0.45\pi/a, -0.33\pi/b)$. The transmission coefficient of the hottest spots in Fig. 2(a) is 1.20. The hot spots in Fig. 2(b) are $k_{\|}$ = ($0.02\pi/a$, $-0.38\pi/b$) and $k_{\|} = (-0.02\pi/a, 0.38\pi/b)$. The transmission coefficient of the hottest spots in Fig. 2(b) is 0.79. A weak transmission of the states in Δ_1 symmetry was observed. In Fig. 2(b), the tunneling feature of multiple states with different symmetry is observed. The transmission spectrum shows obvious tunneling features, with Δ_1 conductance being observed in Fig. 2(b). However, the hot spots in Fig. 2(b) are near the sides. As shown in Fig. S2(c) in the supplementary material, the transmission eigenstate of the majority spin channel in PC also has apparent d-electron feature. In Fig. S2(d) in the supplementary material, the transmission eigenstate of the minority spin channel in PC is similar to a mixture of the s states of Ir, the p states of Se, and the d states of V. This could explain the transmission characteristics of the multiple symmetries in the transmission spectrum in Fig. 2(b). As shown in Fig. 2, the magnitude of the transmission in the PC was also one order of magnitude larger than the transmission in APC, which indicates an obvious TMR effect.

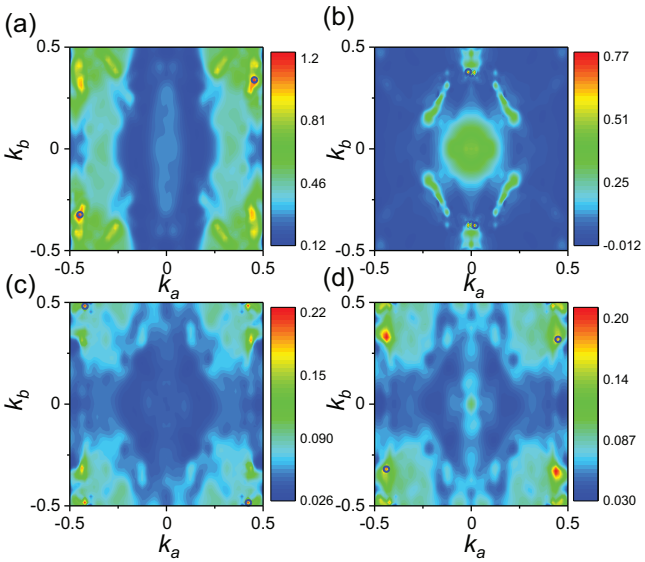


Fig. 2. The $k_{\|} = (k_a, k_b)$ resolved transmission spectra of the Ir/VSe_2/h-BN/VSe_2/Ir MTJs for the (a) majority spin channel and (b) minority spin channel in PC, and the (c) majority spin channel and (d) minority spin channel in APC. The blue circles mark the hottest spots in each figure.

The spin-dependent conductance and the TMR of the MTJs based on VSe_2 and $MnSe_2$ in an equilibrium state are listed in Table 1. From our results in Table 1, we have summarized two methods to increase the TMR of our calculated MTJs. The first method is to select a metal whose work function matches XSe_2 as an electrode. The work functions of the

monolayer $MnSe_2$ and the monolayer VSe_2 calculated by the hybrid functional method are 5.05 eV and 4.99 eV, respectively. In order to ensure that the magnetic properties of the XSe_2 are not affected, only the metal electrodes are strained when building the MTJs structure. The strains on the Ir and Ru electrode when forming the M-XSe_2 interface are listed in Table S1 in the supplementary material. Table 2 displays the work functions (W_m) for the Ir and Ru clean metal when forming the M-XSe_2 interface. The calculation of the work functions of the clean metals in Table 2 considered the strain. Due to the different strains applied to the metal electrode, the work function of the metal forming the interface with different ferromagnets is also different. As shown in Tables 1 and 2, as the difference between the work function of the metal electrode and the work function of the ferromagnetic becomes smaller, the TMR increases. The difference in the work function between the electrode material and the ferromagnet leads to a contact potential difference. The diagram of the band alignment of the M-XSe_2 interface is shown in Fig. S1 in the supplementary material. As shown in Tables 1 and 2, the contact potential difference between the electrode and the ferromagnet has a negative effect on the device performance. Therefore, selecting a metal whose work function that matches the work function of XSe_2 could improve the performance of the device. Another method is to increase the number of layers of h-BN as the barrier layer finitely. When the number of layers of h-BN increases, the conductance is reduced and the TMR increases. We obtain a TMR value of 725.07% when we use a 3.3 Å bilayer h-BN as a barrier. The tunneling process could be simplified into a qualitative model of a free-electron incident on a square barrier of height V_b and thickness d. The transmission could be expressed as $T \sim \exp(-2\kappa d)$.[38,40] The attenuation rate of Bloch state κ can be defined as[38,40]

$$\kappa^2 = \left(\frac{2m}{\hbar^2}\right)(V_b - E_F) + k_{\parallel}^2, \tag{4}$$

where $\hbar$ is the reduced Planck's constant, m is the electron mass, E_F is the Fermi energy, and $k_{\parallel}$ is the wave vector perpendicular to the transport direction. It can be seen from Fig. 3(a) that both the d_{xz} states and the d_{yz} states of the monolayer $MnSe_2$ cross the Fermi level. There are also $d_{x^2-y^2}$ and d_{xy} states that go through the Fermi level with low density of states at the Fermi level. The d_{xz} and d_{yz} states belong to the Δ_5 symmetry, while the $d_{x^2-y^2}$ and d_{xy} states belong to the Δ_2 and $\Delta_{2'}$ symmetries. The transmission hot region of the majority spin in Fig. 1(b) is near the $|k| = 0.5$ line, which is consistent with the symmetry characteristics of these d-state electrons.[40] It can be seen from Fig. 2(b) and Fig. S2(b) in the supplementary material that various electronic states of Ru also participate in the minority spin states tunneling process in the PC. It acts like a background noise that affects the TMR value of the device. The tunneling barrier for Ru's electronic states is the entire $MnSe_2$/h-BN/$MnSe_2$ device layer. The tunneling barrier thickness of the states of the Ru is larger than that of the $MnSe_2$ layer. When the barrier becomes thicker, it can be seen from $T \sim \exp(-2\kappa d)$ that the attenuation of transmission T is exponential with the thickness of the barrier d. Therefore, increasing barrier thickness is more effective in suppressing the transmission of the electronic states of the Ru than the electronic states of the $MnSe_2$. This causes the TMR to become larger when the barrier thickness becomes thicker. However, increasing the thickness of the barrier does not significantly improve the TMR of the MTJs of the VSe_2/h-BN/VSe_2. It can be seen from Fig. 3 that the VSe_2 has states with Δ_1 symmetry through the Fermi level. As shown in Fig. 2(b), there is a characteristic of the Δ_1 symmetry states in the transmission of the minority spin states in the PC state. Therefore, increasing the thickness of the barrier layer does not adequately block the transmission of the VSe_2 electrons with Δ_1 symmetry. This causes the increase of barrier thickness to have little effect on the TMR of VSe_2/h-BN/VSe_2-based MTJs.

Table 1. Conductance of the parallel (G_P) and antiparallel (G_{AP}) configurations of XSe_2 based MTJs. The TMR values of these devices are listed in the last column.

	G_P/Siemens	G_{AP}/Siemens	TMR/%
Ir/$MnSe_2$/1-layer h-BN	4.07×10^{-5}	1.26×10^{-5}	222.72
Ru/$MnSe_2$/1-layer h-BN	2.21×10^{-5}	4.25×10^{-6}	419.94
Ru/$MnSe_2$/2-layer h-BN	1.31×10^{-6}	1.59×10^{-7}	725.07
Ir/VSe_2/1-layer h-BN	1.77×10^{-5}	4.99×10^{-6}	254.48
Ru/VSe_2/1-layer h-BN	7.49×10^{-6}	2.64×10^{-6}	183.55
Ru/VSe_2/2-layer h-BN	3.16×10^{-7}	1.06×10^{-7}	199.15

Table 2. Work functions (W_m) for Ir and Ru clean metal when forming the M-XSe_2 (X = Mn, V; M = Ir, Ru) interface. The strain when forming the interface has been considered.

	W_m of Ir/eV	W_m of Ru/eV
$MnSe_2$	5.60	4.67
VSe_2	5.22	5.34

As the partial density of states (PDOS) shown in Fig. 3, the monolayer $MnSe_2$ and VSe_2 are both metals. Monolayer $MnSe_2$ and monolayer VSe_2 both have d-states that go through the Fermi level. As shown in Figs. 3(c) and 3(d), the d_z^2 states go through the Fermi level in the majority PDOS and minority PDOS. This could explain the presence of the transmission characteristics with Δ_1 symmetry in Fig. 2(b). Furthermore, it can be seen from the spin-resolved PDOS that the $MnSe_2$ exhibits a larger spin polarization than the VSe_2. The results of our DFT+U calculations show that the magnetic moment per unit cell is 3.91 μ_B for $MnSe_2$ and 1.00 μ_B for VSe_2, which is consistent with previous studies.[39] It can be seen from the results in Table 1 that the larger spin polarization of the $MnSe_2$ allows the $MnSe_2$-based MTJs to have a larger TMR than the VSe_2-based MTJs.

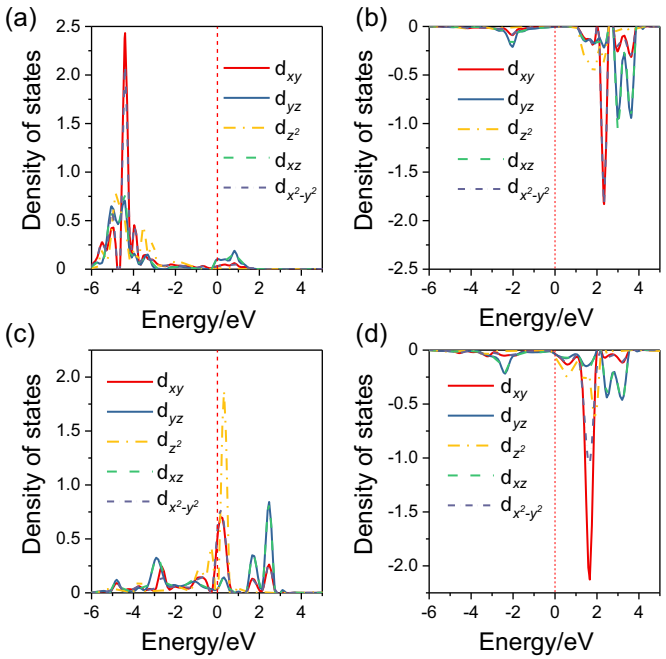


Fig. 3. PDOS of the $MnSe_2$ monolayer for the (a) majority spin states and (b) minority spin states. The Fermi level is set for 0 eV. PDOS of the VSe_2 monolayer for the (c) majority spin states and (d) minority spin states. The Fermi level was set for 0 eV.

As shown in Fig. 4, the non-equilibrium transport properties of the MTJs based on $MnSe_2$ and VSe_2 are calculated by applying a positive bias. In both MTJs, the majority-spin current is larger than the minority-spin current with the increasing bias in the PC. Moreover, in both MTJs, the majority-spin and minority-spin currents changed only slightly with increasing bias in the APC. As the bias voltage increases, the TMR of both MTJs has a small decrease. At the 50 mV bias, the $MnSe_2$-based MTJs still have a TMR of 385%. Additionally, the VSe_2-based MTJs have a TMR of 170% at the 50 mV bias. Our results show that these two MTJs could still work effectively under a finite bias. Previous experimental advances have confirmed that monolayer $MnSe_2$ and VSe_2 have room-temperature ferromagnetism.[26,27] Therefore, it is expected that the TMR of these MTJs can be maintained at room temperature.

To reveal the band diagram of the interface along the transport direction (*c* direction), the projected local density of states (PLDOS) was calculated. The area calculated in Fig. 5 is equivalent to the central area in Fig. 1(a). The region of PLDOS calculated in Fig. 5 corresponds to the central region in Fig. 1. As shown in Fig. 5, the tunneling barrier originating from h-BN can be seen as a dark area at the center of each figure. The single-layer h-BN blocks the overlap of the wave functions of the single-layer $MnSe_2$ on both sides. The Fermi level goes through the valence band in Fig. 5(a), which is consistent with the metallic properties of monolayer $MnSe_2$.

As shown in Fig. 5(a), the Fermi level spans across the majority-spin states of $MnSe_2$ in PC, which indicates a better transmission of the majority-spin states. This means that this device still has an obvious TMR effect. For APC in Figs. 5(c) and 5(d), an obvious dependence of the spin polarization of $MnSe_2$ can be seen in the spin-resolved PLDOS.

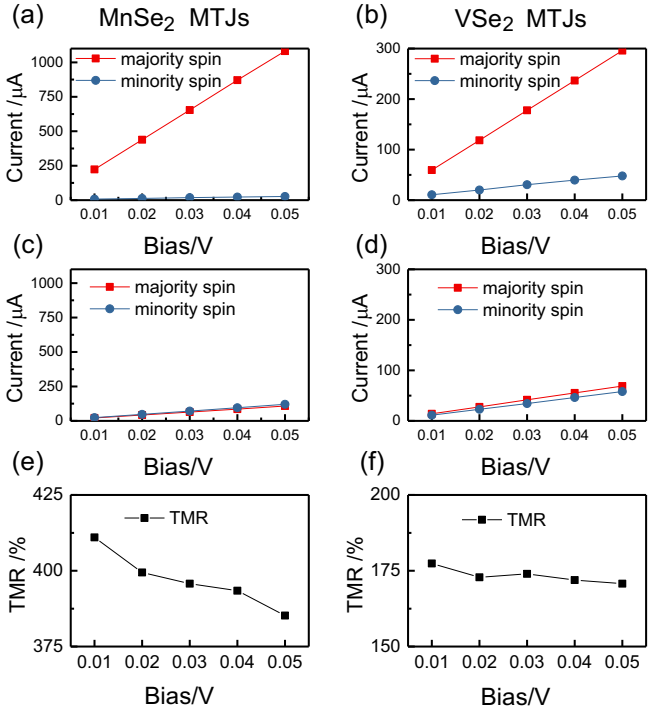


Fig. 4. The left column shows the non-equilibrium transport properties of Ru/$MnSe_2$/h-BN/$MnSe_2$/Ru MTJs. The right column shows the non-equilibrium transport properties of Ru/VSe_2/h-BN/VSe_2/Ru MTJs. The *I*–*V* curves of $MnSe_2$ based MTJs in the (a) PC and (c) APC, the *I*–*V* curves of the VSe_2-based MTJs in the (b) PC and (d) APC. The TMR of the (e) $MnSe_2$-based MTJs and (f) VSe_2-based MTJs.

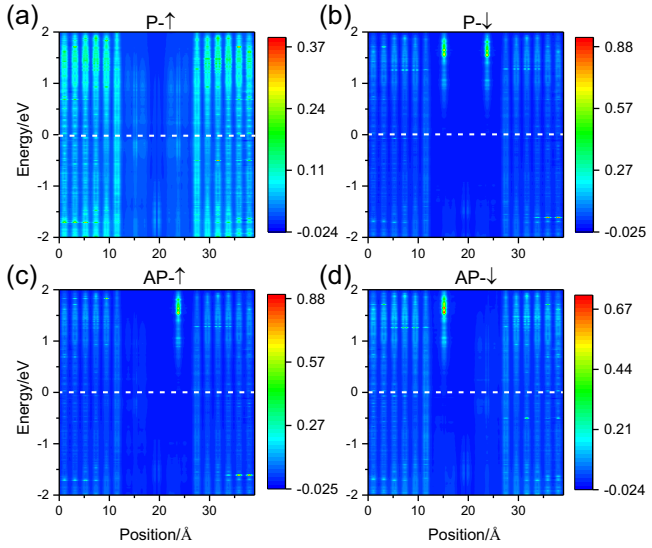


Fig. 5. Projected local density of states along the transport direction (*c* direction) of the Ru/$MnSe_2$/h-BN/$MnSe_2$/Ru MTJs for the (a) majority spin states and (b) minority spin states in PC, and the (c) majority spin states and (d) minority spin states in APC. The Fermi level is indicated by a white dashed line.

4. Conclusion and perspectives

In summary, using *ab initio* calculation, we have studied MTJs based on 2D $MnSe_2$ and VSe_2 with room temper-

ature ferromagnetism. The transmission spectra of majority spin channel and minority spin channel in PC and APC were calculated. We analyzed the transmission characteristics of the transmission spectrum through the electronic structure and orbital composition symmetry of ferromagnetic materials. Based on the results in our paper, we summarized two ways to improve the TMR of our devices: (i) select a metal whose work function matches $X\mathrm{Se}_2$ as an electrode; (ii) increasing the thickness of the barrier within a range of 3.3 Å. We use bilayer h-BN instead of monolayer h-BN as a tunneling barrier. By using bilayer h-BN as tunneling barrier, the TMR of single-layer MnSe_2-based MTJs reaches 725.07%. We further studied the non-equilibrium transport properties of the device by applying positive bias. The results demonstrated that our device still maintained a large TMR under bias. Overall, our study demonstrated that 2D $X\mathrm{Se}_2$ based MTJs with room-temperature ferromagnetism can still maintain a considerable TMR. Therefore, these MTJs would have potential applications in spintronics.

References

[1] Zhang L K, Fang B, Cai J L and Zeng Z M 2018 *Appl. Phys. Lett.* **112** 242408
[2] Wilt J, Goul R, Acharya J, Sakidja R and Wu J Z 2018 *AIP Adv.* **8** 125218
[3] Sun M F, Wang X C and Mi W B 2018 *J. Phys. Chem. C.* **122** 3115
[4] Ma X L, Zhang R J, An C H, Wu S, Hu X D and Liu J 2019 *Chin. Phys. B* **28** 037803
[5] Cao G Y, Zhang C, Wu S L, Ma D and Li X F 2018 *Chin. Phys. B* **27** 124202
[6] Hu S Q, Tian R J, Luo X G, Yin R, Cheng Y C, Zhao J L, Wang X M and Gan X T 2018 *Chin. Phys. B* **27** 128502
[7] Han J Y and Wang J 2019 *Chin. Phys. B* **28** 017103
[8] Piquemal-Banci M, Galceran R, Martin M B, Godel F, Anane A, Petroff F, Dlubak B and Seneor P 2017 *J. Phys. D Appl. Phys.* **50** 203002
[9] Sun Y H, Wang R M and Liu K 2017 *Appl. Phys. Rev.* **4** 011301
[10] Sharma A, Verheijen M A, Wu L F, Karwal S, Vandalon V, Knoops H C M, Sundaram R S, Hofmann J P, Kessels W M M and Bol A A 2018 *Nanoscale* **10** 8615
[11] Karpan V M, Giovannetti G, Khomyakov P A, Talanana M, Starikov A A, Zwierzycki M, van den Brink J, Brocks G and Kelly P J 2007 *Phys. Rev. Lett.* **99** 176602
[12] Piquemal-Banci M, Galceran R, Caneva S, Martin M B, Weatherup R S, Kidambi P R, Bouzehouane K, Xavier S, Anane A, Petroff F, Fert A, Robertson J, Hofmann S, Dlubak B and Seneor P 2016 *Appl. Phys. Lett.* **108** 102404
[13] Pan L F, Huang L, Zhong M Z, Jiang X W, Deng H X, Li J B, Xia J B and Wei Z M 2018 *Nanoscale* **10** 22196
[14] Piquemal-Banci M, Galceran R, Godel F, Caneva S, Martin M B, Weatherup R S, Kidambi P R, Bouzehouane K, Xavier S, Anane A, Petroff F, Fert A, Dubois S M M, Charlier J C, Robertson J, Hofmann S, Dlubak B and Seneor P 2018 *ACS Nano* **12** 4712
[15] Zhou J Q, Qiao J F, Duan C G, Bournel A, Wang K L and Zhao W S 2019 *ACS Appl. Mater. Inter.* **11** 17647
[16] Iqbal M Z, Iqbal M W, Siddique S, Khan M F and Ramay S M 2016 *Sci. Rep.* **6** 21038
[17] Huang B, Clark G, Navarro-Moratalla E, Klein D R, Cheng R, Seyler K L, Zhong D, Schmidgall E, McGuire M A, Cobden D H, Yao W, Xiao D, Jarillo-Herrero P and Xu X D 2017 *Nature* **546** 270
[18] Jiang S W, Shan J and Mak K F 2018 *Nat. Mater.* **17** 406
[19] Song T C, Cai X H, Tu M W Y, Zhang X O, Huang B V, Wilson N P, Seyler K L, Zhu L, Taniguchi T, Watanabe K, McGuire M A, Cobden D H, Xiao D, Yao W and Xu X D 2018 *Science* **360** 1214
[20] Li B, Xing T, Zhong M Z, Huang L, Lei N, Zhang J, Li J B and Wei Z M 2017 *Nat. Commun.* **8** 1958
[21] Gong C, Li L, Li Z L, Ji H W, Stern A, Xia Y, Cao T, Bao W, Wang C Z, Wang Y A, Qiu Z Q, Cava R J, Louie S G, Xia J and Zhang X 2017 *Nature* **546** 265
[22] Kuklin A V, Kuzubov A A, Kovaleva E A, Mikhaleva N S, Tomilin F N, Lee H and Avramov P V 2017 *Nanoscale* **9** 621
[23] Deng Y J, Yu Y J, Song Y C, Zhang J Z, Wang N Z, Sun Z Y, Yi Y F, Wu Y Z, Wu S W, Zhu J Y, Wang J, Chen X H and Zhang Y B 2018 *Nature* **563** 94
[24] Liu S, Yuan X, Zou Y, Sheng Y, Huang C, Zhang E, Ling J, Liu Y, Wang W, Zhang C, Zou J, Wang K and Xiu F 2017 *npj 2D Materials and Applications* **1** 30
[25] Wang Z, Sapkota D, Taniguchi T, Watanabe K, Mandrus D and Morpurgo A F 2018 *Nano Lett.* **18** 4303
[26] Bonilla M, Kolekar S, Ma Y J, Diaz H C, Kalappattil V, Das R, Eggers T, Gutierrez H R, Phan M H and Batzill M 2018 *Nat. Nanotechnol.* **13** 289
[27] O'Hara D J, Zhu T C, Trout A H, Ahmed A S, Luo Y K, Lee C H, Brenner M R, Rajan S, Gupta J A, McComb D W and Kawakami R K 2018 *Nano Lett.* **18** 3125
[28] O'Hara D J, Zhu T C and Kawakami R K 2018 *IEEE Magn. Lett.* **9** 1405805
[29] Brandbyge M, Mozos J L, Ordejon P, Taylor J and Stokbro K 2002 *Phys. Rev. B* **65** 165401
[30] Dudarev S L, Botton G A, Savrasov S Y, Humphreys C J and Sutton A P 1998 *Phys. Rev. B* **57** 1505
[31] Cococcioni M and de Gironcoli S 2005 *Phys. Rev. B* **71** 035105
[32] Giannozzi P, Baroni S, Bonini N, Calandra M, Car R, Cavazzoni C, Ceresoli D, Chiarotti G L, Cococcioni M, Dabo I, Dal Corso A, de Gironcoli S, Fabris S, Fratesi G, Gebauer R, Gerstmann U, Gougoussis C, Kokalj A, Lazzeri M, Martin-Samos L, Marzari N, Mauri F, Mazzarello R, Paolini S, Pasquarello A, Paulatto L, Sbraccia C, Scandolo S, Sclauzero G, Seitsonen A P, Smogunov A, Umari P and Wentzcovitch R M 2009 *J. Phys.: Condens. Mat.* **21** 395502
[33] Grimme S 2004 *J. Comput. Chem.* **25** 1463
[34] Kresse G and Furthmuller J 1996 *Phys. Rev. B* **54** 11169
[35] Kresse G and Furthmuller J 1996 *Comp. Mater. Sci.* **6** 15
[36] Zhang Y K and Yang W T 1998 *Phys. Rev. Lett.* **80** 890
[37] Perdew J P, Burke K and Ernzerhof M 1997 *Phys. Rev. Lett.* **78** 1396
[38] Butler W H, Zhang X G, Schulthess T C and MacLaren J M 2001 *Phys. Rev. B* **63** 054416
[39] Kan M, Adhikari S and Sun Q 2014 *Phys. Chem. Chem. Phys.* **16** 4990
[40] Tiusan C, Greullet F, Hehn M, Montaigne F, Andrieu S and Schuhl A 2007 *J. Phys.-Condens. Mat.* **19** 165201
[41] Bai Z Q, Shen L, Cai Y Q, Wu Q Y, Zeng M G, Han G C and Feng Y P 2014 *New J. Phys.* **16** 103033